Desalination and Water Treatment
www.deswater.com

doi: 10.1080/19443994.2013.778216

51 (2013) 7401–7411
December

Taylor & Francis
Taylor & Francis Group

New combination of solar chimney for power generation and seawater desalination

Nayereh Niroomand, Majid Amidpour*

Faculty of Mechanical Engineering, Department of Energy System Engineering, K.N. Toosi University of Technology, Tehran, Iran
Tel. +98 2184063222; Fax: +98 2188674748; email: amidpour@kntu.ac.ir

Received 6 November 2012; Accepted 17 February 2013

ABSTRACT

In this article, a new combination of solar chimney and Humidification–Dehumidification desalination process is introduced. In this system, the air is humidified by injection of water drops into the air flow. Then, the partial of vapors contained in the air is condensed on the outer surface of the cold water tubes. Two mathematical models have been developed for a one-dimensional flow in the solo solar chimney and the integrated system. The performance of the integrated system including power and potable water production is estimated and the results are discussed. Furthermore, it has been demonstrated that increasing in the temperature and mass flow rate of humidifier inlet water would improve the performance of the integrated system. It is found that the increase in water production would cause the decrease in power output. Also, to produce more fresh water, the number of dehumidifier tubes should be increased.

Keywords: Solar chimney; Power production; Seawater desalination; Humidifier; Dehumidifier

1. Introduction

Energy crisis and fresh water shortage are two issues which humans confront especially in deserted regions. Fossil fuels are the most common fuels which are used to produce electricity and fresh water. As the usage of fossil energies has induced negative effects on the environment and nearly exhausted, a great interest has been devoted to use of the renewable energies to produce both power and fresh water. Making use of solar energy as a clean energy, especially in a sunny region, and setting up a combined model of solar chimney and desalination system can be a good choice to overcome the aforementioned problems to some extent.

Over 70% of the earth is covered by water but only 3% of all these sources are fresh water, and just less than 1% of fresh water is accessible for human direct use, so there is a great pressure on the fresh water resources [1]. In recent years, human solved this problem by desalinating of brackish water. There are many methods for desalting salt water. In seawater desalination systems, both fossil fuels and renewable energies can be used [1]. Various studies have been done on the utilization of the solar energy among the renewable energies. Solar desalination by humidification and dehumidification (HD) of air has been received considerable attention lately. Several pilots of

*Corresponding author.

HD system have been constructed in Jordan [2], Malaysia [3], and Tones [4]. Most of investigations have been done for optimization the performance of HD process [5,6]. Dawoud et al. [7] studied the possibility of cooling techniques for the condenser of seawater greenhouse desalination based on air humidification–dehumidification. Alhazmy [8] presented a theoretical analysis based on the second law of thermodynamics for estimating the minimum work required for air dehumidification process to produce potable water in a humidification–dehumidification desalination cycle. Mahmoudi et al. [9] studied the feasibility of using wind energy to power brackish water greenhouse desalination units proposed for the development of the southern region of the case study country of Algeria.

Moreover, solar chimney is a promising large-scale power technology that absorbs direct and diffused solar radiation and produces power without releasing greenhouse gases. The earliest modern day reference to a solar tower concept appears in a German book by Günther and de Haas [10]. In 1983, basic idea, construction and power generation principles of the solar tower were discussed by Haaf et al. [11]. They described the operation of the system and presented results of a prototype solar chimney power plant built in Manzanares, Spain. This prototype had a chimney with 194.6 m height, a collector with 122 m in radius and a single vertical axis turbine. This model operated with the peak power about 50 kW for eight years [12]. Since then many researchers have studied the feasibility of the large scale solar chimney [13,14]. Several pilots of solar chimney have been constructed in the world and their performance has been investigated [15–19]. However, the solar chimney has low conversion efficiency, it compensates for this disadvantage by its cheap, simple technology and low maintenance cost.

The concept of combination of solar chimney and seawater desalination was proposed by Kashiwa in 2006 for the first time [20]. Kashiwa introduced a theoretical basis for the feasibility of the Solar Cyclone, suggesting that an experimental study of the separation device would be worthwhile. Akbarzadeh et al. [21] suggested the utilization of a solar pond instead of collector in the solar chimney and built a small model of that. The thermal energy that stored at the bottom of the solar pond is used in a heat exchanger to heat up the air. Moreover, the use of a direct contact heat exchanger is suggested where fresh water production is desired. Zhou et al. [22] proposed a combined solar chimney system (CSCS) for both power generation and seawater desalination. In the combined system, the dry ambient air becomes warm and saturated when it flows through a layer of seawater drawn from the adjacent sea. Vapors in the air were condensed to fresh water in a high-efficiency condenser installed at the chimney outlet. For this model, a vast pond should be constructed that it made it difficult to access the turbine and chimney for maintenance purpose. Zou et al. [23] compared the performance of the solo solar chimney (SSC) and CSCS for power generation and seawater desalination. They proposed a new solar chimney system combined with solar still desalination. Through the theoretical analysis, it has been demonstrated that the integrated system would significantly improve the solar energy utilization efficiency as well as the land resources utilization efficiency. Zuo et al. [24] have built a small-scale experimental device for the integrated solar chimney with solar still. Its performance has been studied based on the practical weather condition. They concluded that the integrated system can achieve simultaneously the multi-targeted production, such as power and freshwater.

The HD process operates at low temperature and the total required energy can be obtained from the solar energy, so it is suitable to combine with solar chimney. To the authors' knowledge, there is no general study on the combination of the solar chimney and HD process. In the present research work, the combination of solar chimney and HD process has been investigated. In this model, there is no need to build a vast pond or many solar stills. The area under the collector roof can be used as a greenhouse for agricultural uses that in other combined models is impossible. In this work, based on mathematical analysis, the performances of the SSC and CSCS have been evaluated. Through the analysis, the role of the humidifier inlet water temperature and mass flow rate on the power and water desalinated production and dehumidifier area have been investigated. Also, the influence of increasing power output on the water desalinated production has been studied.

2. Description of CSCS

The CSCS schematic is shown in Fig. 1. The combined solar chimney model consists of five major parts, including collector, chimney, wind turbine, humidifier and dehumidifier. The humidifier consists of water nozzles which arrange in an annular direction in the collector inlet. The dehumidifier is assumed as the cross-flow vertical tubes bank which allows cold brine water passes through them. Similar to nozzles, dehumidifier tubes arranged in the annular direction.

When warm water is sprayed into the ambient air, the simultaneous interphase heat and mass transfer

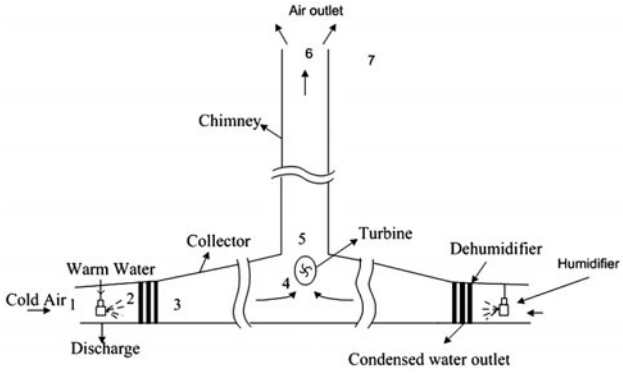

Fig. 1. Schematic diagram of CSSC.

will occur between the air and drops. If the water temperature is greater than that of the ambient air, the air flow becomes warm and humid. Then, warm and wet air passes through the dehumidifier, and condensation of the water vapor from the air stream takes place on the outer surface of the vertical tubes. Then, the air flow is heated up through the collector and its velocity and temperature increase. The air in the chimney base is warmer than the ambient air which results in an updraft air flow in the chimney. The kinetic energy of the air flow is converted into mechanical energy by pressure-staged wind turbine at the base of the chimney and into electrical energy by generators. This model is very suitable for the regions adjacent to the sea or power plants which produce warm water as discharge.

3. Mathematical model and principle description

Two mathematical models based on energy balance equations of various components of the system are developed: one for SSC and the other for combined model. To simplify the analysis, the following assumptions are made:

(1) The air follows the ideal gas law.
(2) The process in the humidifier and dehumidifier is operating under adiabatic and steady conditions.
(3) Vertical gradient of temperature in the collector and humidifier is neglected.
(4) The stable meteorological conditions are assumed to exist.

In this article, the ambient temperature and pressure are considered as 290 K, 101,325 Pa and the relative humidity of the air is equal to 30%. The solar radiation is taken as 1,000 W/m^2.

3.1. Performance analysis of solar chimney

One-dimensional equations of the energy balance for a control volume of the collector which contains radius r to $r+\Delta r$ (as shown in Fig. 2) can be expressed as follows

For air flow,

$$h_c(T_c - T_a) + h_g(T_g - T_a) = \frac{c_p \dot{m}_a}{2\pi r}\frac{\partial T_a}{\partial r} \tag{1}$$

For collector roof,

$$\alpha_c I + h_{r,cg}(T_g - T_c) = h_A(T_c - T_{atm}) + h_{rs}(T_c - T_{sky}) + h_c(T_c - T_a) \tag{2}$$

For ground surface,

$$\alpha_g \tau_c I = h_g(T_g - T_a) + h_l(T_g - T_{g,0}) + h_{r,cg}(T_g - T_c) \tag{3}$$

In Eqs. (1)–(3), h_g and h_c are convection heat transfer coefficients, h_{rs} and $h_{r,cg}$ are radiation heat transfer coefficients, h_l is conduction heat transfer coefficient.

The convection heat transfer coefficients are functions of the Reynolds and the Grashof numbers. The heat transfer coefficient between the collector roof and the fluid flowing through the collector is [25]

$$h_c = \left(\left(Nu_a\frac{\lambda_a}{2H_c}\right)^4 + \left(Nu_c\frac{\lambda_a}{H_c}\right)^4\right)^{0.25} \tag{4}$$

The heat transfer coefficient between the surface of earth and the fluid flowing through the collector is [25]

$$h_g = \left(\left(Nu_a\frac{\lambda_a}{2H_c}\right)^4 + \left(Nu_g\frac{\lambda_a}{H_c}\right)^4\right)^{0.25} \tag{5}$$

It should be noted that the surface of the ground is considered adiabatic, so h_g is equal to zero. Then,

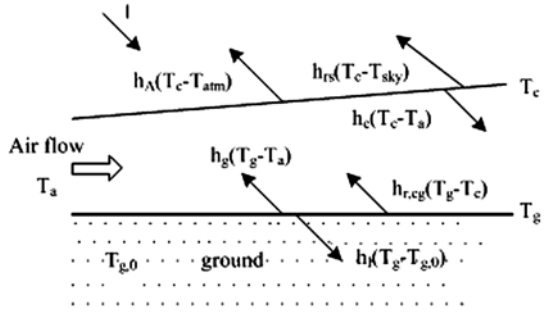

Fig. 2. Energy flow through a control volume in collector.

increasing in the air temperature through the collector can be calculated by Eqs. (1)–(3).

The driving force that caused air to flow through the solar chimney is due to a pressure difference between a column of cold air outside and a column of hot air inside the chimney [26]. The driving force is given by

$$\Delta P_{\text{tot}} = g \int_0^{H_{\text{ch}}} (\rho_{\text{atm}} - \rho_{\text{ch}}) dH \tag{6}$$

The pressure drop depends on the difference between density of air in chimney base and the ambient in the same altitude. By increasing the air temperature in the collector, the pressure difference would be increased.

The pressure difference is consumed by three parts, static component (the pressure drop at the turbine), dynamic (the kinetic energy of the airflow) component and the friction losses in the chimney

$$\Delta P_{\text{tot}} = \Delta P_{\text{s}} + \Delta P_{\text{d}} + \Delta P_{\text{f}} \tag{7}$$

$$\Delta P_{\text{d}} = \frac{1}{2}\rho_6 V_6^2 \tag{8}$$

$$\Delta P_{\text{f}} = f\frac{L}{d}\frac{\rho}{2}V^2 \tag{9}$$

where the wall friction factor f was calculated using the Colebrook formula for the shear stress in chimney [26].

Power generated by the turbine can be expressed as:

$$P_{\text{e}} = \eta_{\text{tg}} \Delta p_{\text{s}} V_{\text{avg}} \tag{10}$$

where V_{avg} is the average volumetric flow rate through the turbine.

In this article, the efficiency of the turbine generator is recommended by other researchers as 80% [27].

3.2. Solar chimney integrated with HD desalination

3.2.1. Analysis of humidifier

In the humidifier, water droplets interact with the air and the heat and mass transfer occur in the interface of the water droplets and air stream in horizontal parallel flow. The outlet temperature and humidity ratio of the air in the humidifier depend on the inlet air and water conditions. It is assumed that all drops have the same behavior in the system and the drops leave the nozzles in the same horizontal velocity with the same diameter (Fig. 3).

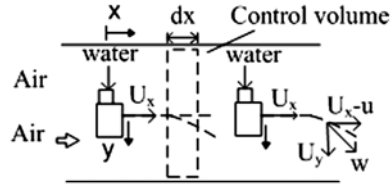

Fig. 3. Humidifier model schematic.

The humidification process is modeled by dividing humidifier length into several sections and solving the mass and heat transfer equations for each section. The inlet air temperature and humidity ratio of each section is set equal to the outlet conditions of the previous section. The initial conditions of the first section are set equal to the ambient air conditions. By this procedure, the temperature and humidity ratio of the air in the humidifier outlet can be determined.

Increase in the air humidity ratio occurs due to the evaporation of the water droplet in the air.

$$\frac{d\omega}{dx} = \frac{A_{\text{s}} h_{\text{m}} n(\omega_{\text{i}} - \omega)}{u U_{\text{x}}} \tag{11}$$

where ω_{i} is humidity ratio of the air in the surface of water drop and h_{m} is mass transfer coefficient for drops.

Mass loss of the water drops occurred due to evaporation can be expressed as:

$$\frac{dm_{\text{d}}}{dx} = \frac{-\rho_{\text{a}} A_{\text{s}} h_{\text{m}} (\omega_{\text{i}} - \omega)}{U_{\text{x}}} \tag{12}$$

Then, the variation of the drop diameter can be calculated by

$$\frac{dD}{dx} = \frac{-2\rho_{\text{a}} h_m (\omega_{\text{i}} - \omega)}{U_{\text{x}} \rho_{\text{w}}} \tag{13}$$

Changing in the air temperature is related to the heat and mass transfer from drops which can be assumed as follows:

$$\dot{m}_{\text{a}} U_{\text{x}} \frac{dh_{\text{a}}}{dx} = -NhA_{\text{s}}(T_{\text{a}} - T_{\text{d}}) - Nh_{\text{fg}} U_{\text{x}} \frac{dm_{\text{d}}}{dx} \tag{14}$$

The energy balance of water droplet represented the drop temperature change as below:

$$\frac{d(m_{\text{d}} h_{\text{d}})}{dx} = \frac{hA_{\text{s}}(T_{\text{a}} - T_{\text{d}})}{U_{\text{x}}} + h_{\text{fg}} \frac{dm_{\text{d}}}{dx} \tag{15}$$

The x- and y-momentum equations for drops in the parallel flow are given below [28]:

$$\frac{dU_x}{dx} = -\frac{0.75C_D\rho_a W(U_x - u)}{U_x\rho_d D} - \frac{3U_x}{D}\frac{dD}{dx} \tag{16}$$

$$\frac{dU_y}{dx} = \frac{g(\rho_d - \rho_a)}{U_x\rho_d} - \frac{0.75C_D\rho_a WU_y}{U_x\rho_d D} - \frac{3U_y}{D}\frac{dD}{dx} \tag{17}$$

In this work, drops are assumed as rigid body; therefore, the drag coefficient depends on the Reynolds number. Drag coefficient can be written as calculated in Ref. [28].

Reynolds number is calculated based on the velocity of drops relative air that is expressed as [29]:

$$\mathrm{Re}_d = \frac{\rho_a WD}{\mu_a} \tag{18}$$

$$W = \sqrt{(U_x - u)^2 + U_y^2} \tag{19}$$

The number of the water droplets per second produced by nozzles can be calculated by the following relation [30]:

$$N = \frac{6\dot{m}_w}{\pi d^3\rho_w} \tag{20}$$

The mass and heat transfer coefficients have been determined based on the following relations [28]:

$$Sh = \frac{h_m D}{D} = 2 + 0.6\mathrm{Re}^{0.5}Sc^{0.33} \tag{21}$$

and

$$Nu = \frac{h_a D}{\lambda_a} = 2.0 + 0.6\mathrm{Re}_d^{0.5}\mathrm{Pr}^{1/3} \tag{22}$$

where D is diffusivity coefficient of water vapor in air, and Sc is Schmidt number.

Air flow in the collector can be humidified in several steps. In this work, humidity ratio of air increases in three steps in the humidifier.

3.2.2. Condensation in dehumidifier

To describe the heat balance and the rate of heat transfer in the dehumidifier, the following equations are used [31].

Equation of energy balance in dehumidifier are given in below relation

$$\dot{m}_a(h_{a,3} - h_{a,2}) = \dot{m}_w C_{p,w}(T_{c,out} - T_{c,in}) \tag{23}$$

The dehumidifier heat transfer area can be calculated by

$$\dot{m}_w C_{p,w}(T_{c,out} - T_{c,in}) = U_c A_c \mathrm{LMTD}_c \tag{24}$$

where (log mean temperature difference) LMTD would be computed under the assumption of counter flow condition. The appropriate form of LMTD in cross-flow heat exchanger is obtained by applying correction factor to the value of LMTD [31]

$$\mathrm{LMTD}_c = F \times \mathrm{LMTD} \tag{25}$$

So, the total number of tube banks, N_t, could be calculated by:

$$N_t = \frac{A_c}{\pi D_o L_t} \tag{26}$$

where L_t is assumed equal to the height of the collector roof.

A general expression for overall heat transfer coefficient based on external area is given by [31]:

$$\frac{1}{U_c} = \frac{1}{h_o} + \frac{r_o}{r_i h_i} + \frac{r_o \ln(r_o/r_i)}{k_w} \tag{27}$$

In Eq. (27), h_o and h_i denote the heat transfer coefficients on the air side and the heat transfer coefficient on the water side [32,33].

All properties of the air stream and water are calculated according to the relations used in Ref. [34].

The fresh water production rate in tube banks is calculated by [31]:

$$\dot{m}_{pw} = \dot{m}_a(\omega_{a,2} - \omega_{a,3}) \tag{28}$$

It is considered that the dehumidifier outlet air is saturated, so the humidity ratio is the function of the temperature as following equation [31]:

$$\omega = 2.19 \times 10^{-6}T^3 - 1.85 \times 10^{-4}T^2 + 7.06 \times 10^{-3}T^2 - 0.077 \tag{29}$$

The pressure drop for the flow over tube banks is calculated by the following equation [35]:

$$\Delta P_{cond} = \frac{1}{2} f N_{row} V^2 \tag{30}$$

The friction factor, f, for tubes in-line configuration is given by Ref. [36]. N_{row} is demonstrated the number

of tube rows, which could be calculated by considering the distance between tubes in a row, S_T, spacing between the tube in different rows, S_L, and the total number of tubes.

V in Eq. (30), is reference velocity based on the minimum area, which determined by the following equation [37]:

$$V = u\frac{S_T}{(S_T - D_o)} \tag{31}$$

where u is denoted the air velocity in the empty channel. S_T and D_o are assumed as transversal pitch and tube outside diameter.

Reynolds number is calculated by following relation

$$\mathrm{Re} = \frac{VD_o}{v} \tag{32}$$

It can be seen that the pressure drop decrease with decreasing air velocity. As the air velocity increases through the collector, the nearest place of the collector entrance after the humidifier is the best placement of the dehumidifier.

3.2.3. Power output in CSCS

In combined model, the term of pressure drop across the dehumidifier tubes is added to terms of pressure drops. So, the turbine pressure drop is solved by:

$$\Delta P_s = \Delta P_{tot} - \Delta P_d - \Delta P_f - \Delta P_{cond} \tag{33}$$

To maximize the power production, the pressure drop in the turbine should be increased which results in minimizing of pressure losses.

4. Results and discussion

The performance of the SSC and the integrated system are analyzed by using mathematical modeling. Table 1 shows the parameters which are used for the calculation, and the results of the calculation are tabulated in Table 2. It can be seen that 87.45 kW produced from the turbine in SSC. Considering the adiabatic assumption for the ground surface, this value is not far from the 50 kW output reported in Manzanares in Spain [12].

For the integrated system with the same dimension introduced by Zuo et al. [23], the water production flow rate is estimated about $8.8\,\mathrm{kg\,s^{-1}}$. As shown in Table 2, the fresh water production in this work is about $8.5\,\mathrm{kg\,s^{-1}}$ which could be improved. It will be explained in the following sections. So, it is competitive in comparison with results derived by Zuo.

As indicated in Table 2, the power output of CSSC is less than that of a SSC with the same dimension, but the difference between them is not remarkable. It is shown that the temperature and mass flow rate of the collector outlet airflow for CSSC is less than SSC. The reason is the air humidity ratio in the whole integrated system is more than SSC. Since water has a lower molecular weight, the moisture content of the air flowing in the integrated system results in a lower air density. So, as shown in Table 2, despite of lower mass flow rate, the air velocity of the collector outlet in CSSC is more than SSC. The increase in the air velocity might result in a shorter time for the air inside the collector to absorb energy while passing through the collector. Thereby, the outlet temperature for the CSSC would become less than the corresponding temperature for the SSC. As a result, the power output of CSSC is less than SSC.

Table 1
Values of design and operating parameters

Parameter	Symbol	Value	Parameter	Symbol	Value
Outer collector radius/m	r_a	120	Outer diameter of dehumidifier tube/m	D_0	0.04
Inner collector radius/m	r_i	13	Inner diameter of dehumidifier tube/m	D_i	$0.85\,D_0$
Chimney height/m	H_{ch}	194	Longitudinal pitch/m	s_l	0.2
Chimney diameter/m	d_{ch}	10.08	Thermal conductivity of condenser tubes/ $\mathrm{kW\,m^{-1}\,K^{-1}}$	K_W	0.04
Mean collector roof height/m	H_c	1.7			
Horizontal velocity of drops/ m/s	U_x	5	Number of Tubes rows	N	1–10
Humidifier inlet water temperature/ ℃	$T_{w,in}$	40	Cooling water temperature /℃	$T_{c,in}$	18
			Humidifier inlet water mass flow rate/$\mathrm{kg\,s^{-1}}$	$\dot{m}_{w,h}$	1,300
Transverse pitch/m	S_T	1.4			

Table 2
Performance of proposed SSC and CSSC

Parameters	Value	Parameters	Value
Collector outlet airflowtemperature (SSC)/℃	45.7	Collector outlet airflow temperature (CSSC)/℃	45
Collector outlet airflow velocity (SSC)/m s^{-1}	6.05	Collector outlet airflow velocity (CSSC)/m s^{-1}	6.2
Turbine pressure drop (SSC)/Pa	122	Humidifier outlet airflow temperature (CSSC)/℃	28
Total pressure difference (SSC)/Pa	185	Total pressure difference (CSSC)/Pa	183
Power output (SSC)/kW	87.45	Power output (CSSC)/kW	84
Mass flow rate of dry air (SSC)/kg s^{-1}	928	Mass flow rate of dry air (CSSC)/kg s^{-1}	906
		Fresh water productivity (CSSC)/kg s^{-1}	8.5

4.1. Effect of water production on power output

Fig. 4 shows that the power output declines by increasing water production while the length of humidifier is assumed constant. To desalinate more seawater as Eq. (28), ω_3 should decrease. Hence, as the air humidity ratio is dependent on the air temperature, DBT of dehumidifier outlet would decrease, while ambient temperature is constant. By decreasing T_3, the collector outlet air temperature reduces and as a consequence the driving force declines. So the power output would decrease. Also, to achieve more fresh water production, the required heat transfer area of the dehumidifier would be increased. Because the lengths of tubes are the same as collector roof height, the number of tubes should be increased.

4.2. Effect of humidifier inlet water temperature

In Fig. 5, the maximum fresh water which can be desalinated in dehumidifier is shown. By growth in $T_{w,hi,}$ the temperature difference between air and water would increase. This caused the increase in $T_{a,2}$ and $\omega_{a,2}$ as it is visible in Fig. 6. Hence, the amount of water vapor carried by the air flow would increase. If the required heat transfer area is provided, the amount of water production will achieve to its maximum value, which affects the $T_{a,3}$. To compare the

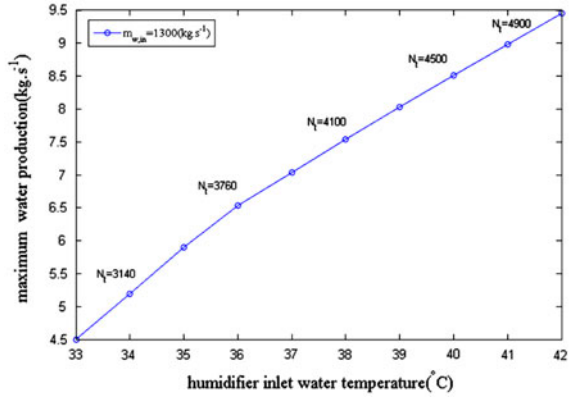

Fig. 5. Maximum water production vs. humidifier water temperature.

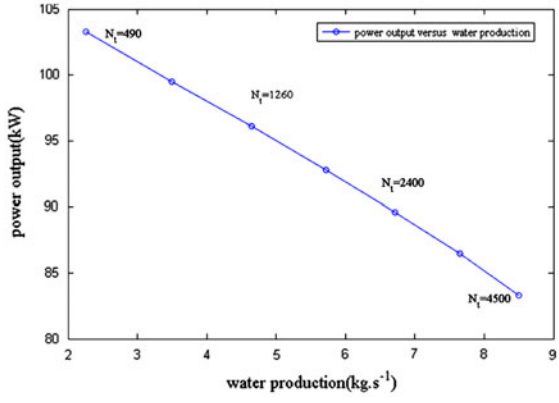

Fig. 4. Power output vs. maximum water production.

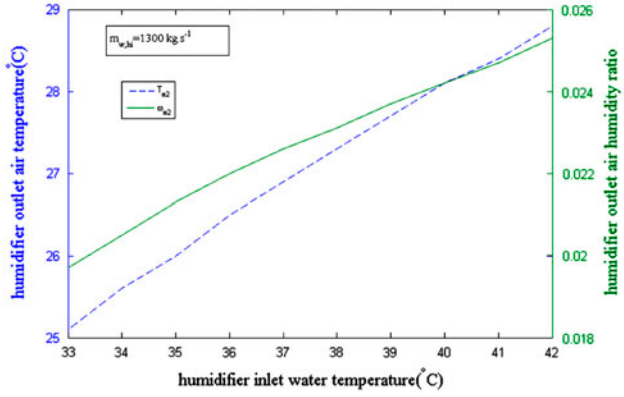

Fig. 6. Humidifier outlet air temperature and humidity ratio.

maximum of the water production, it is assumed that $T_{a,3}$ is constant (equal to 20°C). As it is demonstrated in Fig. 5, the amount of maximum water production could be achieved to the maximum value of 9.5 kg s^{-1} from a low value of 4.5 kg s^{-1}, by variation in $T_{w,hi}$, from 33 to 42°C. Also, the number of tubes has to increase from the value of 3,140 to the value of 4,900.

If N_c does not supply the required heat transfer area in the dehumidifier, the maximum water production could not occur. For this case, the result is depicted in Fig. 7 for three values of N_c. It is found that the number of dehumidifier tubes has significant effect on water production. By increasing in N_c, the water production rate could be close to its maximum value. For example, for the case of $T_{w,hi}$ of 42°C, the amount of water production is 5.5 kg s^{-1} when N_c is equal to 1,500, while its maximum value is 9.5 kg s^{-1}, which indicates the high sensitivity of the water production to the number of dehumidifier tubes. When the maximum water production does not occur, the temperature rise in humidifier that caused by escalating of $T_{w,hi}$ would improve the performance of the collector. As a result, the power production could enhance with increase in $T_{w,hi}$, as shown in Fig. 8. It is seen that the decrement in N_c would increase the power output due to the growth of T_{a3}. On the other hand, when maximum water production does not occur, T_{a3} would be higher than its specified value (20°C). So more reduction in N_c results in higher air temperature at dehumidifier outlet. That it is caused an increase in power production.

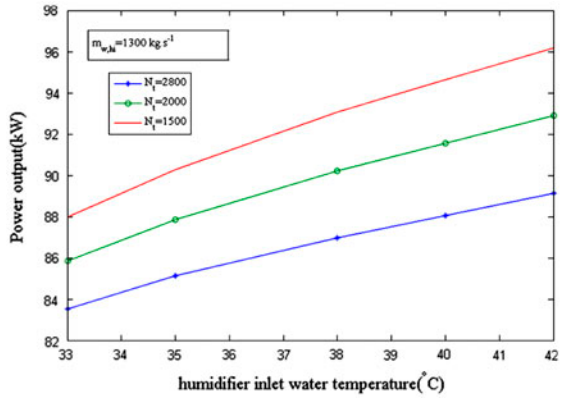

Fig. 8. Power outlet vs. humidifier water temperature.

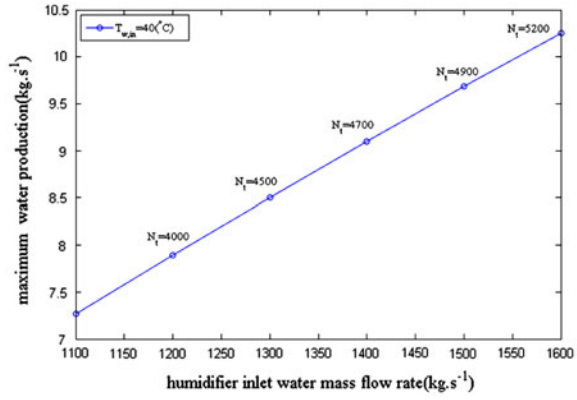

Fig. 9. Maximum water production vs. humidifier inlet water mass flow rate.

4.3. Effect of humidifier inlet water mass flow rate

Fig. 9 shows the effect of humidifier inlet water mass flow on the maximum water production. By growing of water mass flow, the number of drops in the air will increase. It means the overall contact area between water drops and air will increase. As a result, the air temperature and humidity ratio at the humidifier outlet will increase. So water production will increase if the required dehumidifier heat transfer area is provided.

As explained before, when the number of the dehumidifier tubes does not supply the required heat transfer area to achieve the maximum water production, T_{a3} will increase. This causes an increase in power production as shown in Fig. 10. The trend of variation of power output, in Figs. 8 and 10 is similar. It indicates an increase in both $T_{w,hi}$ and $m_{w,hi}$ improved power production.

As shown in Fig. 11, the amount of water production increases by growth of $m_{w,hi}$, but its value is less than the maximum water production. It is found that by increasing in N_c, its value becomes close to the maximum water production.

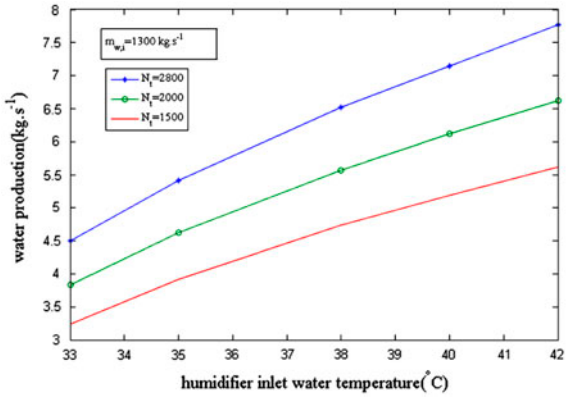

Fig. 7. Water production vs. humidifier water temperature.

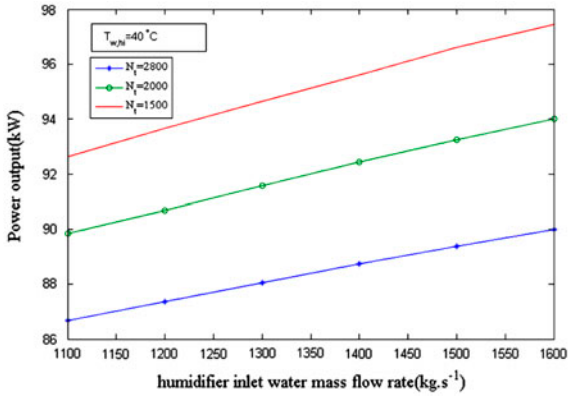

Fig. 10. Power production vs. humidifier inlet water mass flow rate.

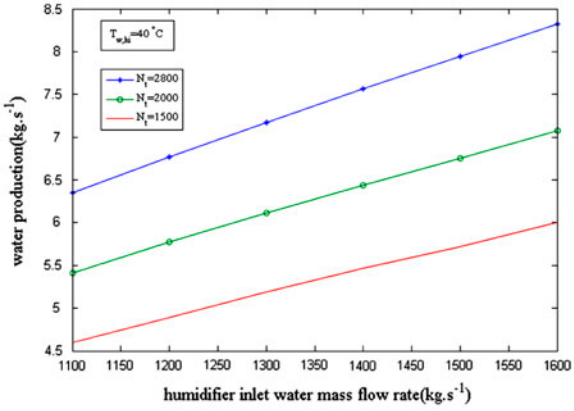

Fig. 11. Water production vs. humidifier inlet water mass flow rate.

5. Conclusion

In this paper, the concept of combination of a solar chimney with HD system has been assessed. Two mathematical models have been developed to analyze the performance of SSC and CSSC. The following conclusions can be drawn from the analyses.

- The results indicate that the power output of CSSC is just 3.9%(3.45 kW) less than SSC, meanwhile the integrated system desalinate 8.5 kg s^{-1} fresh water, which can be the advantage of this combination.
- In some cases, not only the combination of seawater desalination by solar chimney does not decrease power output, but also it could improve it to some extent.
- By desalting more water, power output will decrease.
- The number of dehumidifier tubes has a significant effect on the power output and distillate flow rate.
- The temperature and mass flow rate of the humidifier inlet water have effects on the performance of the system. To increase both power and water desalinate production, growth of humidifier inlet water temperature and mass flow rate could be beneficial.

Nomenclature

A_s	—	surface area of drops, m^2
C_P	—	heat capacity, J kg^{-1} K^{-1}
D	—	diameter, m
f	—	friction coefficient
g	—	gravitational acceleration, m s^{-2}
H	—	height, m
h	—	enthalpy, J kg^{-1} or convection heat transfer coefficient, W m^{-2} K^{-1}
h_{fg}	—	enthalpy of evaporation, J kg^{-1}
h_m	—	mass transfer coefficient
L	—	length, m
m	—	mass flow rate, kg s^{-1}
N	—	number of drops per second
n	—	number of drops per second per unit cross-section area of humidifier
Nu	—	Nusselt number
I	—	solar radiation, W m^{-2}
r	—	radius, m
Sh	—	Sherwood number
T	—	temperature, K or °C
U	—	drop velocity, m s^{-1}
u	—	air flow velocity, m s^{-1}
V	—	velocity, m s^{-1}
W	—	relative velocity of drop relative to air, m s^{-1}

Greek symbols

α	—	absorptivity thermal diffusivity, m^2 s^{-1}
Δp_{cond}	—	condenser or dehumidifier pressure drop
Δp_d	—	dynamic pressure drop, Pa
Δp_s	—	pressure drop across the turbine (static pressure drop), Pa
Δp_{tot}	—	total pressure difference in the chimney, Pa
λ	—	thermal conductivity, W m^{-1} k^{-1}
ε	—	emissivity
η	—	efficiency
ρ	—	density, kg m^{-3}
σ	—	Stefan–Boltzmann constant, 5.67×10^{-8}, W m^{-2} K^{-4}
τ:	—	transmissivity
φ	—	relative humidity
ω	—	humidity ratio

Subscripts

A	—	ambient
a	—	air
atm	—	atmosphere

ave — average
c — collector or condenser (dehumidifier)
ch — chimney
d — drop
g — ground
hi — humidifier inlet
i — interface, inlet or inner surface
o — outlet or outer surface
r — radiation
s — sky
tg — turbine generator
v — vapor
w — water, wall
x — coordinate
y — coordinate
1 — humidifier inlet
2 — humidifier outlet/dehumidifier inlet
3 — dehumidifier outlet/collector inlet
4 — collector outlet
5 — chimney inlet
6 — chimney outlet
7 — atmosphere

References

[1] S.A. Kalogirou, Seawater desalination using renewable energy sources, Prog. Energy Combust. Sci. 31 (2005) 242–281.
[2] N.K. Nawayseh, M.M. Farid, A.Z. Omar, S. Al-Hallaj, A.R. Tamimi, A simulation study to improve the performance of a desalination unit constructed in Jordan, Desalination 109 (1997) 277–284.
[3] N.K. Nawayseh, M.M. Farid, S. Al-Hallaj, A.R. Tamimi, Solar desalination based on humidification process: I. Evaluating the heat and mass transfer coefficients, Energy Convers. Manage. 40 (1999) 1423–1439.
[4] B. Bacha, H. Maalej, A.Y. Ben Dhia, H. Ulber, I. Uchtmann, H. Engelhardt, J. Krelle, Perspectives of solar powered desalination with the SMCEC technique, Desalination 122 (1999) 177–183.
[5] S.M. Soufari, M. Zamen, M. Amidpour, Performance optimization of the humidification–dehumidification desalination process using mathematical programming, Desalination 237 (2009) 305–317.
[6] H. Muller-Holst, M. Engelhardt, W. Scholkopf, Small-scale thermal seawater desalination simulation and optimization of system design, Desalination 122 (1999) 255–262.
[7] B. Dawoud, Y.H. Zurigat, B. Klitzing, T. Aldoss, G. Theodoridis, On the possible techniques to cool the condenser of seawater greenhouses, Desalination 195 (2006) 119–140.
[8] M.M. Alhazmy, Minimum work requirement for water production in humidification–dehumidification desalination cycle, Desalination 214 (2007) 102–111.
[9] H. Mahmoudi, N. Spahis, M.F. Goosen, S. Sablani, S.A. Abdul-wahab, N. Ghaffoure, N. Drouiche, Assessment of wind energy to power solar brackish water greenhouse desalination units: A case study from Algeria, Renew. Sustain. Energy Rev. 13 (2009) 2149–2155.
[10] H. Günther, W. de Haas, Die künftige Energieversorgung der Welt [Energy for the Future of the World], Franck'sche Verlagshandlung, Stuttgart, 1931.
[11] W. Haaf, K. Friedrich, G. Mayr, J. Schlaich, Solar chimneys, part I: Principle and construction of the pilot plant in Manzanares, Sol. Energy 2 (1983) 3–20.
[12] W. Haaf, Solar chimneys, part II: Preliminary test results from the Manzanares pilot plant, Sol. Energy 2 (1984) 141–161.
[13] S. Nizetic, N. Ninic, B. Klarin, Analysis and feasibility of implementing solar chimney power plants in the Mediterranean region, Energy 33 (2008) 1680–1690.
[14] M. Tingzhen, L. Wei, X. Guoling, X. Yanbin, G. Xuhu, P. Yuan, Numerical simulation of the solar chimney power plant systems coupled with turbine, Renew. Energy 33(5) (2008) 897–905.
[15] X. Zhou, J. Yang, B. Xiao, G. Hou, Simulation of a pilot solar chimney thermal power generating equipment, Renewable Energy 32 (2007) 1637–1644.
[16] H. Kulunk, A prototype solar convection chimney operated under Izmit conditions, in: T.N. Veziroglu (Ed.), Proceedings of Seventh MICAES, 1985, 162.
[17] A.B. Kasaeian, E. Heidari, Sh. Nasiri Vatan, Experimental investigation of climate effects on the efficiency of a solar chimney pilot power plant, Renewable Sustainable Energy Rev. 15 (2011) 5202–5206.
[18] C. Ketlogetswe, J.K. Fiszdon, O.O. Seabe, Solar chimney power generation project–The case for Botswana, Renewable Sustainable Energy Rev. 12 (2008) 2005–2012.
[19] C.B. Maia, A.G. Ferreira, R.M. Valle, M.F.B. Cortez, Theoretical evaluation of the influence of geometric parameters and materials on the behavior of the airflow in a solar chimney, Comput. Fluids 38 (2009) 625–636.
[20] B.A. Kashiwa, C.B. Kashiwa, The solar cyclone: A solar chimney for harvesting atmospheric water, Energy 33 (2008) 331–339.
[21] A. Akbarzadeh, P. Johnson, R. Singh, Examining potential benefits of combining a chimney with a salinity gradient solar pond for production of power in salt affected areas, Sol. Energy 83 (2009) 1345–1359.
[22] X. Zhou, B. Xiao, W. Liu, X. Guo, J. Yang, J. Fan, Comparison of classical solar chimney power system and combined solar chimney system for power generation and seawater desalination, Desalination 250 (2010) 249–256.
[23] L. Zuo, Y. Zheng, Z. Li, Y. Sha, Solar chimneys integrated with sea water desalination, Desalination 276 (2011) 207–213.
[24] L. Zuo, Y. Yuan, Z. Li, Y. Zheng, Experimental research on solar chimneys integrated with seawater desalination under practical weather condition, Desalination 298 (2012) 22–33.
[25] R. Sangi, M. Amidpour, B. Hosseinizadeh, Modeling and numerical simulation of solar chimney power plants, Sol. Energy 85 (2011) 829–838.
[26] M.A. Bernardes, A. Voss, G. Weinrebe, Thermal and technical analyses of solar chimneys, Sol. Energy 75 (2003) 511–524.
[27] A.J. Gannon, T.W. von Backstrom, Solar chimney cycle analysis with system loss and solar collector performance, Sol. Energy Eng. 122 (2000) 133–137.
[28] S.S. Kachhwaha, P.L. Dhar, S.R. Kale, Experimental studies and numerical simulation of evaporative of air with a water spray- I. Horizontal parallel flow, Heat Mass Transfer 41(2) (1998) 447–464.
[29] Z. Xu, Y. Xiao, Y. Wang, Experimental and theoretical studies on air humidification by a water spray at elevated pressure, Appl. Therm. Eng. 27 (2007) 2549–2558.
[30] R. Sureshkumar, S.R. Kale, P.L. Dhar, Heat and mass transfer processes between a water spray and ambient air – II. Simulations, Appl. Therm. Eng. 28 (2008) 361–371.
[31] M. Mehrgoo, M. Amidpour, Derivation of optimal geometry of a multi-effect humidification–dehumidification desalination unit: A constructal design, Desalination 281 (2011) 234–242.
[32] Incropera, DeWitt, Bergman and Lavine, Fundamentals of Heat and Mass Transfer, Wiley Publication, New York, NY, 2007.
[33] D. Sajjan, T. Karlsson, L. Vanmling, Reasons for drop in shell and tube condenser performance when replacing R22 with zeotropic mixtures. Part 1. Analysis of experimental findings, Refrig. 27 (2004) 552–560.
[34] M. Al-Sahali, H.M. Ettouney, Humidification dehumidification desalination process: Design and performance evaluation, Chem. Eng. 143 (2008) 257–264.

[35] E.M. Sparrow, S.S. Kang, Longitudinally-finned cross-flow tube banks and their heat transfer and pressure drop characteristics, Heat Mass Transfer 28(2) (1985) 339–350.
[36] A. Kosar, C. Mishra, Y. Peles, Laminar flow across a bank of low aspect ratio micro pin fins, Fluids Eng. 127 (2005) 419–430.
[37] A.A.M. Hassan, Effect of tube arrangement and condensate flow rate on the pressure loss for cross flow of steam in small tube bundle, Energy Convers. Manage. 51 (2010) 703–709.